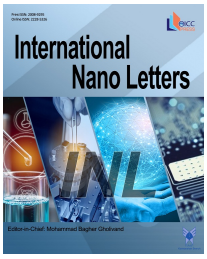

Volume 14, Issue 2, 142407 (1-10)

International Nano Letters (INL)

https://doi.org/10.57647/inl.2024.1402.07

Nanotechnology-Enhanced Polymer Scaffolds with Antibacterial and Angiogenic Properties on Diabetic Wound Healing

Hayder Sudan Abbas Obaid[1,2], Fateme Mirzajani[1,3,*], Amin Hamidi[1], Iliya Fattahiyan[3], Meysam Omidi[1]

[1] *Protein Research Center, Shahid Beheshti University, Tehran, Iran.*
[2] *Department of Medical, Hammurabi College of Medicine, University of Babylon, Hillah, Iraq.*
[3] *Faculty of Life Sciences and Biotechnology, Shahid Beheshti University, Tehran, Iran.*

[*]**Corresponding author:** f_mirzajani@sbu.ac.ir, and fateme.mirzajani@gmail.com

Original Research

Abstract:

Healing of wounds is a complicated and coordinated process with four phases, namely control of bleeding, inflammation, growth, and regeneration. Chemokines, growth inhibitors, and growth factors are all vital in establishing cell-cell contacts and the extracellular matrix. The conventional therapies include herbal treatments, specialist dressings, and interim scaffolds. Polymer scaffolds are a new innovation in wound treatment, providing a three-dimensional, temporary scaffolding for biological activities during healing. Objectives: A study attempted to speed wound healing processes by combining angiogenesis-stimulating protein (VEGF), vitamin D, silver carbon quantum dot (Ag-CQD), and henna extract (*Lawsonia inermis*) on polymeric nanostructures. Characteristics of the manufactured nanostructure investigated using scanning electron microscopy (SEM), Fourier-transform infrared attenuated total reflectance spectroscopy (FT-IR ATR), and X-ray Powder Diffraction (XRD). The release of Lawson and VEGF (Vascular endothelial growth factor) was measured using high-performance liquid chromatography (HPLC) and nanodrop micro-volume spectrophotometers. The nanostructures were further strengthened by immobilizing VEGF to increase angiogenesis at the wound site. Vitamin D and lawsone exhibited more than 70% favorable benefits on wound healing phases. Also silver nanoparticles demonstrate significant antibacterial activity against gram-positive and gram-negative bacteria. In terms of antibacterial efficacy, this scaffold was evaluated against Staphylococcus aureus and Escherichia coli, and the scaffold Gel/Chi/Pcl/AgCQD/Law/VEGF with $175-200$ nm fibers and 10 mg of Lawson was shown to be stable at pH $= 7.4$. Thus, the produced scaffold exhibited considerable resistance against *S. aureus*, and chitosan mixed with Lawson material appeared to be extremely promising in wound healing.

Keywords:

Smart nanostructure; *Lawsonia inermis* L.; VEGF; Wound Healing; Vitamin D; Ag-CQD

Cite this article: Obaid, H.S.A., Mirzajani, F., Hamidi, A., Fattahiyan, I., Omidi, M. Nanotechnology-Enhanced Polymer Scaffolds with Antibacterial and Angiogenic Properties on Diabetic Wound Healing. *Int. Nano Lett.* **14**(2), 142407 (2024).

1. Introduction

Diabetes mellitus (DM) is a serious condition that impacts practically all bodily systems, with the foot being the most adversely impacted region, resulting in diabetic foot ulcer (DFU), the most fatal consequence of DM [1]. Diabetic foot ulcers frequently arise from two chronic consequences of diabetes: Peripheral neuropathy and peripheral vascular disease, which may be exacerbated by infection and might ultimately lead to major or minor amputation [2]. Traumatic injuries are generally classified as chronic or acute, based upon their pathogenesis and impact. Acute wounds may be healed by a sequence of molecular reactions, whereas chronic wounds tend to create ulcers, especially in diabetic patients [3]. Ischemic and arterial ulcers caused by inadequate blood flow to the wound area, neuropathic ulcers due to neuropathy, and neuro ischemic ulcers, which are caused by both neuropathy and ischemia [4]. Wound healing has four stages: Hemostasis, inflammation, proliferation, and remodeling. After a wound, there is vasoconstriction along with plug formation by platelets [5]. Later, blood clots are

formed to control bleeding. This is followed by the inflammation stage where white blood cells such as macrophages and neutrophils arrive at the injury site, clearing pathogens and debris through phagocytosis [6]. Macrophages get engaged in wound healing through the presence of two phenotypes: M1 (pro-inflammatory) and M2 (pro-healing). These are antibacterial activity, and the secretion of pro-angiogenic factors such as cytokines and growth factors for the purpose of angiogenesis [7].

Diabetes can cause several problems, such as neuropathy, poor circulation, and increased risk of infection in different stages of wound healing. In the normal process of wound healing, approximately 80% of macrophages in the wound have an M1 pro-inflammatory phenotype, which later switches to around 80% − 85% anti-inflammatory M2 macrophages [8]. In diabetic cases, hyperglycemia may result in dysregulation of M1 macrophage polarization, leading to a prolonged inflammatory phase [9]. Various advanced therapies such as pressure off-loading, Negative pressure wound therapy (NPWT), debridement, pathogenic suppression, and application of Hydrogels, advanced bandages, and dressings are meant to accelerate the healing process by moisture balance, infection prevention, and medical optimization of comorbidities such as peripheral vascular disease, nicotine use, and blood glucose control [10].

Vascular endothelial growth factor (VEGF) also plays a role in fetal and adult blood vessel formation and wound healing. VEGF is also responsible for the induction of angiogenesis and lymphangiogenesis in diabetic patients and, therefore, wound healing [11]. It also improves re-epithelialization, keratinocyte proliferation, and ECM (Extracellular matrix) generation [12]. Traditional medicine and herbal extracts, such as green tea, *Curcuma longa*, and *aloe vera*, have a long-standing history of use in diabetic wound treatments, connecting us to the rich heritage of wound care. *Curcuma longa* [13], *aloe vera* [14] have been employed for decades in diabetic wound healing. *Lawsonia inermis* (henna) is a quickening agent in wound healing due to its antibacterial, anti-inflammatory, and antioxidant activities. This is attributed to a number of bioactive molecules like flavonoids, quinones, tannins, epicatechin, and catechin, which render henna useful in wound healing [15]. Also nanomaterials, with their significant potential for delivering drugs topically and promoting cell proliferation, vascularization, and cell signaling, are paving the way for a promising future in wound care [16]. Nanomaterials are the ideal dressings that mimic the ECM and have antimicrobial properties.The application of polymeric nano-scaffolds accelerates wound healing by promoting angiogenesis [17]. Adding graphene oxide to this approach provide mechanical properties like conductivity, as well as enhancing immune regulation, biocompatibility, promoting stem cell differentiation, and antioxidant features. These additional benefits could significantly enhance the effectiveness of the wound healing process, making the proposed solution even more promising [18].

In this study, a polymeric nano-scaffold enriched with Ag-CQD and egg shell has been used with VEGF protein and *Lawsonia inermis* extracts to observe its effect on the healing of diabetic wounds.

2. Experimental

2.1 Design and synthesis of polymer scaffolds

Polymer scaffolds were produced from α-TCP (Alpha tricalcium phosphate) that was pre-prepared using crushed eggshells, Ag-CQD nanoparticles, and henna extract. The crushed eggshells were first washed with deionized water, followed by mechanical surface abrasion using fine-grade sandpaper and later sterilized by phosphate buffer solution treatment or by UV sterilization. α-TCP synthesis involved dissolving 2 g of eggshell powder in orthophosphoric acid, mixed for 24 hours, 6000 rpm centrifuged, and dried out the fraction settled. A 5% chitosan (Sigma Aldrich Co., Germany) in 2% acetic acid was mixed with 5% ascorbic acid (Sigma Aldrich Co., Germany) and subsequently 0.3 g of silver nitrate and 0.1 g of sodium hydroxide were added; the resulting solution, subjected to hydrothermal treatment at 150 °C for 24 minutes, was filtered to produce a yellow Ag-CQD solution. Henna extract was obtained by dissolving 50 g of dried leaves in 500 mL of aqueous-ethanol (Zakaria Co., Iran) solution and undergoing ultrasonic extraction for 15 minutes. The extract was centrifuged, filtered, and vacuum-dried under a solvent. Ethanol was employed to remove color compounds and chlorophyll to purify the extract, and the active ingredient, lawsone, which remained, was freeze-dried into powder form. Scaffolds were prepared by a mixture of solutions containing silver nanoparticles, chitosan, vitamin D, and lawsone extract (figure 1 C). These mixtures were poured into 25-well plates, frozen in liquid nitrogen, and exposed to freeze drying for the removal of the solvent, and thus, scaffolds were ready for further application.

2.2 Biological effectiveness evaluations

Biological assays were performed to evaluate the antibacterial efficacy, cytocompatibility, and wound healing capabilities of the synthesized scaffolds and Ag-CQD. To assess potential bacterial contamination on sterilized eggshells, Muller Hinton broth (3.6%) with agar (1.9%) was placed in sterilized Petri dishes, into which sterilized eggshells were added. The Petri dishes were then incubated at 37 °C for 18 − 24 h to observe bacterial proliferation. For the antibacterial evaluation of Ag-CQD using the inhibitory zone (disc diffusion) test, suspensions of *Escherichia coli* and *Staphylococcus aureus* were produced and diluted to the 0.5 McFarland standard. The bacterial solution was subsequently distributed uniformly onto Muller Hinton agar (2.1%) with the lawn culture method. Wells were established and Ag-CQD was introduced, subsequently incubated at 37 °C for 24 h. The sizes of the inhibitory zones were compared with tetracycline and gentamicin, serving as positive controls for Gram-positive and Gram-negative bacteria, respectively [19]. To assess the antibacterial efficacy of the constructed scaffolds, the samples were submerged in nutrient broth injected with the specified bacterial strains. Following incubation at 37 °C for 18–24 hours, bacterial growth suppression was assessed using UV-Vis spectrophotometer absorbance at 610 nm at different time intervals.

The minimum inhibitory concentration (MIC) of Ag-CQD was ascertained by combining 50 µL of bacterial culture with 50 µL of successive dilutions of Ag-CQD (ranging from 0.5% to 100%) in microplate wells, followed by incubation and measurement of absorbance at 625 nm. For the cytotoxicity experiment, scaffolds were sterilized in 75% ethanol for 12 hours, and L929 fibroblast cells were cultured in RPMI (Roswell Park Memorial Institute medium) media supplemented with 10% FBS (Fetal bovine serum) and 1% penicillin. Approximately 1×10^5 cells were inoculated onto each scaffold and incubated for 48 hours. The MTT (Methylthiazolyldiphenyl-tetrazolium bromide for cell viability assays) test was employed to evaluate cell viability [20]. The *in vivo* healing capacity of the scaffolds was assessed using male rats with a mean weight of $30-35$ g, where excisional full-thickness wounds were induced. There are 10 analysis groups in the experiment. The groups consist of one non-treated control group and three treatments: eggshell extract, vitamin D, and silver-carbon quantum dots (Ag-CQD). All three treatment concentrations (0.5%, 2%, and 5%) were tested at three-time intervals, i.e., four days, eight days, and twelve days post-treatment. The scaffolds were treated on the wounds, and healing was evaluated on day 4, day 8, and day 12. Tissue was harvested after treatment and was stained using Masson's trichrome for collagen deposition and epidermal regeneration. Rats were anesthetized with subcutaneous administration of 0.05 mL ketamine and xylazine and two full-thickness wounds, each rat having a diameter of 1 cm with a punch on the back of the rats. To induce diabetes in rats as per earlier references [21], one of the usual practices is administering Streptozotocin (STZ-55 mg/kg, administered intraperitoneally once after a 12 h fasting period), a cytotoxin specific for β-cells. Following $12-16$ h fasting schedule (water only), STZ is freshly prepared in 0.1 M cold citrate buffer (pH 4.5) and administered intraperitoneally with 55 mg/kg body weight. This results in selective β-cell killing of the pancreas and hyperglycemia. Rats typically develop diabetic glucose levels ($\geq$ 250 mg/dL) within 72 h. Each experimental group included six rats ($n = 6$), chosen based on similar body weights and health status. The sample size was determined according to previous studies with comparable designs to ensure statistical validity. Glucose levels are assayed by tail vein blood samples. 5% glucose in drinking water for 24 h after injection guards against initial hypoglycemic shock. At the end of the experimental period, the animals were sacrificed humanely by an overdose of sodium pentobarbital ($>$ 100 mg/kg, i.p.), following standard ethical procedure for the care and use of laboratory animals [21–23]. A standard commercial wound dressing containing silver sulfadiazine (1%) was used as a positive control to compare healing efficacy with the experimental scaffolds. Data were analyzed using one-way ANOVA followed by Tukey's post hoc test, with $p < 0.05$ considered statistically significant. All analyses were performed using GraphPad Prism 9.

3. Results

3.1 Antibacterial activity of Ag-CQDs and scaffolds

The antibacterial effectiveness of produced Ag-CQD nanoparticles against two model pathogens, *Staphylococcus aureus* (Gram-positive) and *Escherichia coli* (Gram-negative), was assessed using a disc diffusion experiment. The results demonstrated enhanced antibacterial efficacy of Ag-CQDs against Gram-positive bacteria [24]. The zone of inhibition for *S. aureus* was recorded at 4.9 mm, whereas for *E. coli*, it was 3.9 mm (figures 1 A and 1 B). The disparity arises from the characteristics of bacterial cell walls; specifically, Gram-negative bacteria have an extra outer membrane abundant in lipopolysaccharides, which might diminish the permeability of Ag-CQDs, hence impeding their antibacterial efficacy. The MIC values of Ag-CQDs against *S. aureus* and *E. coli* were ascertained using the broth microdilution technique, ranging from 0.5% to 100%. Both strains demonstrated identical sensitivity to Ag-CQDs, with a minimum inhibitory concentration (MIC) of 0.165 mg/mL. This indicates the modest antibacterial efficacy of Ag-CQDs, suggesting that a larger concentration may be necessary to completely eradicate germs in more intricate systems. Ag-CQD-loaded scaffolds were evaluated for antibacterial efficacy following a 24-h incubation in bacterial cultures. Contrary to the predictions of prior investigations, supplementation with more than 150 mg/mL Ag-CQD did not improve bacterial inhibition. Scaffolds with 0.5% Ag-CQD demonstrated optimal antibacterial activity, but higher concentrations ($150-200$ mg/mL) diminished antibacterial efficacy (figures 1 A and 1 B).

This discrepancy is likely attributable to potential interactions between Ag-CQDs and other components of the scaffolds (e.g., chitosan, plant extract, α-TCP) that cause agglomeration or impede the release of active molecules.

3.2 Scaffold physiochemical characteristics

Particle size distribution and zeta potential were measured using dynamic light scattering (DLS), while morphology and dispersion were confirmed via scanning electron microscopy (SEM). The degradation patterns of the synthesized scaffolds were monitored under two pH conditions (5.4 and 7.4) for a duration of 144 hours (figures 2 A and 2 B). Scaffolds No.1 and No.2 exhibited rapid degradation within 24 hours under both pH conditions. Scaffolds No.3 to No.6 demonstrated mechanical stability for 6 days; however, Scaffold No.4 (containing 0.5% Ag-CQD) displayed a moderate and appropriate degradation rate compared to the others. Notably, as the concentrations of Ag-CQDs (2% and 5%) increased, the degradation rate diminished, potentially attributable to enhanced cross-linking or agglomeration of nanoparticles within the matrix. The liberation of lawsone from scaffolds was assessed using UV-Vis spectrophotometry in PBS solutions at pH levels of 7.4 and 5.4 (figures 2 C and 2 D). Scaffold No.3, composed of chitosan, plant extract, eggshell, vitamin D, and 0.5% Ag-CQD, demonstrated optimal release efficiency at both pH levels. Elevated concentrations of Ag-CQD resulted in diminished release of extracts, potentially attributable to decreased porosity or interactions between Ag-CQDs and scaffold components

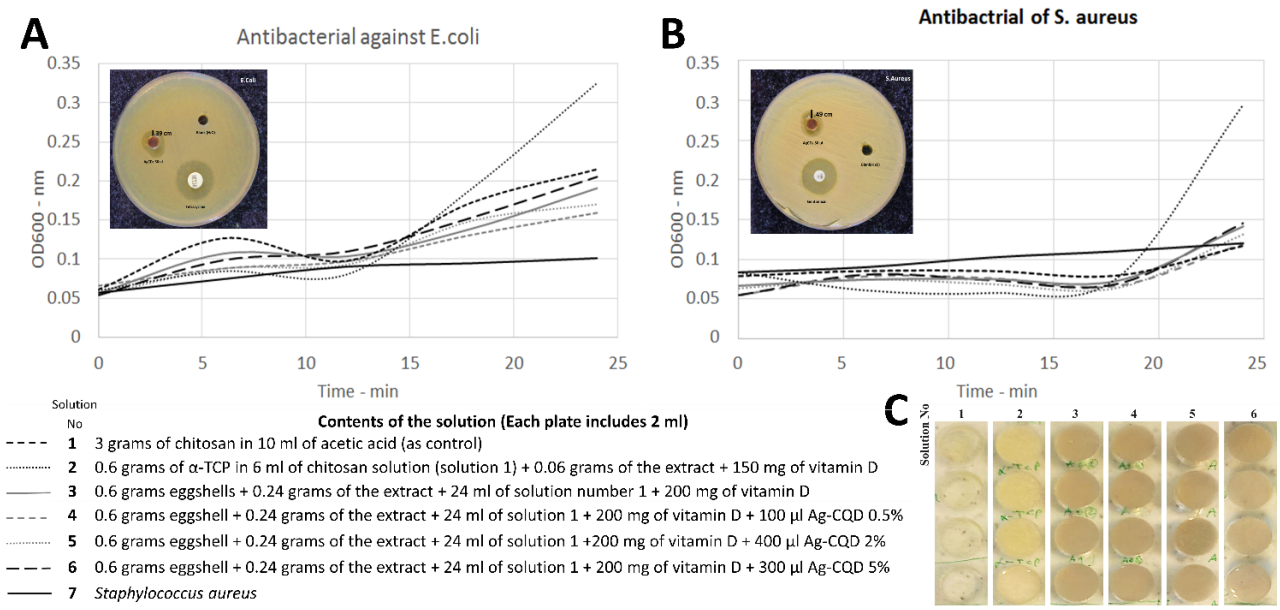

Figure 1. The ability of different scaffolds to inhibit (A) *Escherichia coli* and (B) *Staphylococcus aureus* cells over a 24-hour period. The plates depicted in both graphs are from the Ag-CQD antibacterial assay using the Inhibition Zone (Disc Diffusion) method. (C) 25 plates containing different solutions mentioned on table 1 before being placed in the freeze dryer.

that impede extract diffusion. SEM imaging validated the porous morphology of the scaffolds (figure 2 E-2 J). Pure chitosan scaffolds exhibited elevated pore density and increased pore diameters. The incorporation of α-TCP, plant extract, and Ag-CQD resulted in a noticeable decrease in both the quantity and dimensions of pores. Scaffold No.4 (0.5% Ag-CQD) exhibited an ideal pore architecture characterized by appropriately sized and uniformly distributed pores. However, an excess of Ag-CQD led to pore collapse and diminished porosity, potentially explaining the decline in antibacterial efficacy and extract release efficiency at elevated Ag-CQD concentrations.

Figure 3 depicts the ATR-FTIR spectra for different compositions of chitosan, carbon dots, phosphoric acid, silver nanoparticles, α-TCP, eggshell, vitamin D, and plant extracts. The spectra are utilized to ascertain the functional groups present in the chemical structures. The broad band in the $4000-3000\ cm^{-1}$ region is ascribed to O-H stretching, a characteristic of chitosan, plant extracts, and vitamin D. The $3000-2800\ cm^{-1}$ area consists of C-H stretching vibrations, indicating the existence of alkane groups in organic compounds. The $1800-1500\ cm^{-1}$ area exhibits the distinctive bands corresponding to the stretching of C=O and C=C, present in vitamin D, plant extracts, and chitosan modifications. The $1500-1000\ cm^{-1}$ area encompasses C-N, N-O, and C-O stretching, linked to polysaccharides and phosphate compounds such as α-TCP. Peaks are seen at $1000-500\ cm^{-1}$ corresponding to ring structures, silver-related interactions, and silicon bonds. In the left section (3A-3D), acetic acid chitosan (3A) exhibits pronounced O-H and amide bands, carbon dot chitosan (3B) introduces supplementary C=C vibrations, the chitosan-eggshell-vitamin D-H_3PO_4 complex (3C) displays phosphate-associated bands, and the chitosan-eggshell-vitamin D-plant extract sample (3D) contains additional organic functional groups. The right half (3E-3G) illustrates the influence of silver nanoparticles (3E), exhibiting increased intensity in the $1400-1000\ cm^{-1}$ range, maybe attributable to Ag-chitosan interactions. The spectra containing α-TCP (3F, 3G) exhibit intensified phosphate bands between $1100-900\ cm^{-1}$, corroborating the interactions between chitosan and α-TCP. The spectrum fluctuations affirm the effective integration of various components, emphasizing their interrelations, which might enhance the biological and mechanical features of the final composites.

Figure 4 displays the X-ray diffraction (XRD) patterns of the produced scaffolds, illustrating the structural alterations generated by different additions. The original chitosan scaffold (Fig. 4 A) has a prominent peak at around $2\theta \approx 20°$, indicating its highly amorphous structure, in accordance with the disordered arrangement of chitosan chains. The incorporation of α-TCP, vitamin D, and plant extract (Fig. 4 B) reveals distinct diffraction peaks between 25° and 35°, indicative of the crystalline α-TCP phase. Chitosan exhibits some crystallinity while maintaining its overall amorphous characteristics. The scaffold infused with eggshell-derived calcium, vitamin D, and plant extracts (Fig. 4 C) exhibits larger and less strong peaks in the same region, indicative of weakly crystalline eggshell calcium carbonate and phosphate species.

The α-TCP-loaded scaffold has reduced peak intensity and heightened dispersion, confirming the existence of less-ordered crystalline phases in this formulation. The introduction of Ag-CQDs at varied concentrations (Fig. 4 D-4 F) results in the emergence of additional diffraction peaks at roughly 38°, 44°, 64°, and 77°, corresponding to the (111), (200), (220), and (311) planes of the face-centered cubic (FCC) crystalline structure of metallic silver. The prominence and intensity of these peaks are significantly heightened in the Ag-CQD2 sample (Fig. 4 E), signify-

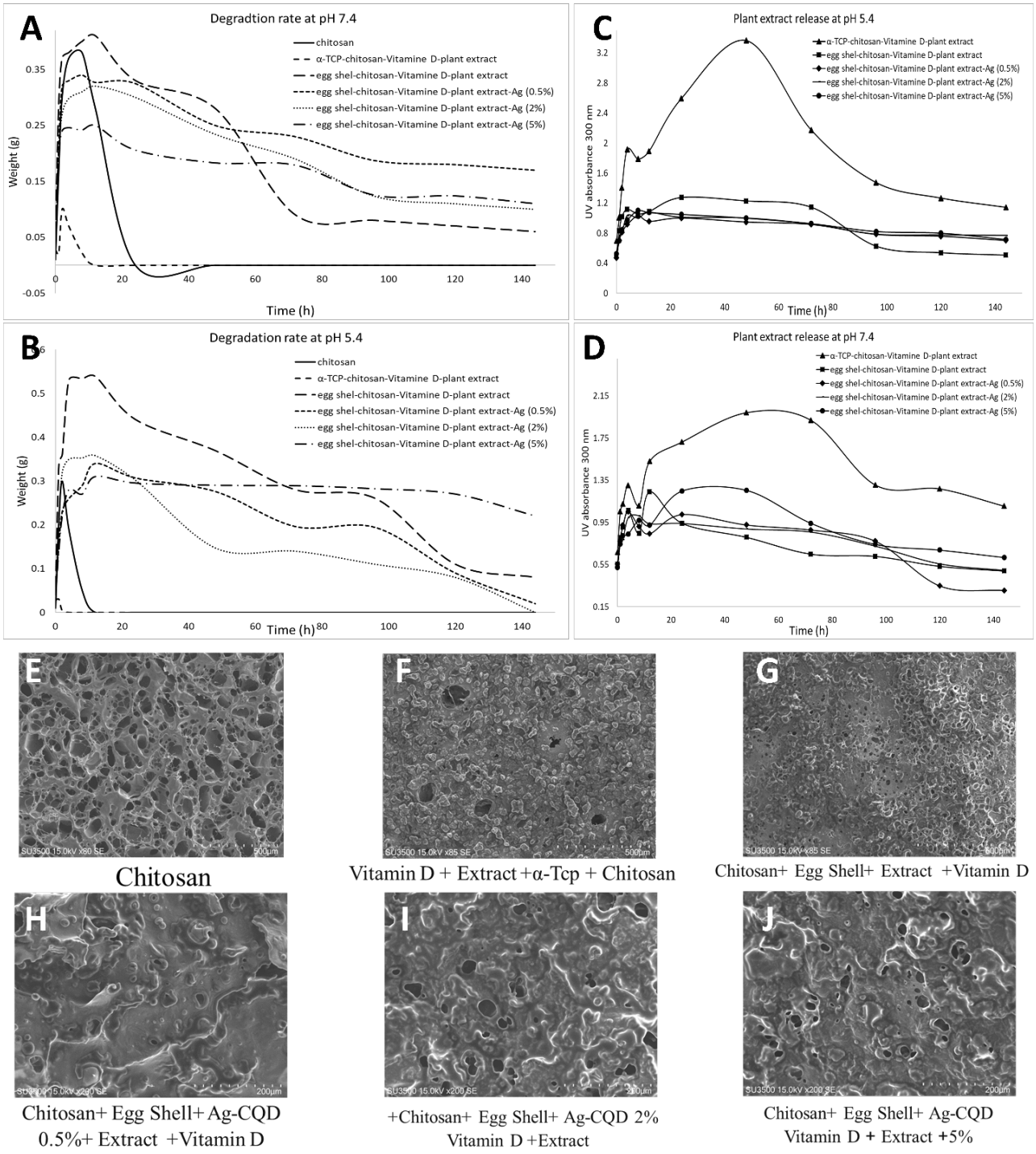

Figure 2. Degradation rate of scaffolds in 144 h at (A) 7.4 pH and (B) 5.4 pH. Graph of plant extract release rate from synthesized scaffolds at (C) 7.4 pH and (D) 5.4 pH and SEM images of synthesized scaffolds (E-J).

ing higher loading and improved crystallinity of Ag-CQDs. In the Ag-CQD3 sample (Fig. 4 F), there is a progressive decrease in peak intensity, likely attributable to improved dispersion and less agglomeration of the nanoparticles at elevated concentrations. Notwithstanding these structural alterations, the prominent peak at $2\theta = 20°$ persists in all samples, indicating that the amorphous nature of the chitosan scaffold is preserved throughout all formulations. The retained amorphous nature is appropriate for scaffold applications, since it is flexible, biodegradable, and possesses enough drug-loading capacity.

3.3 Cytocompatibility and *in vivo* wound healing assessment

L929 fibroblast cell viability studies demonstrated that the vitality of all scaffolds was exceedingly high (> 97%).Scaffold No.3 (control, devoid of Ag-CQDs) had the greatest viability at 99.03%. The viability was diminished by a little degree (99.01%) with the incorporation of 0.5% Ag-CQDs, although remained within acceptable limits. Ele-

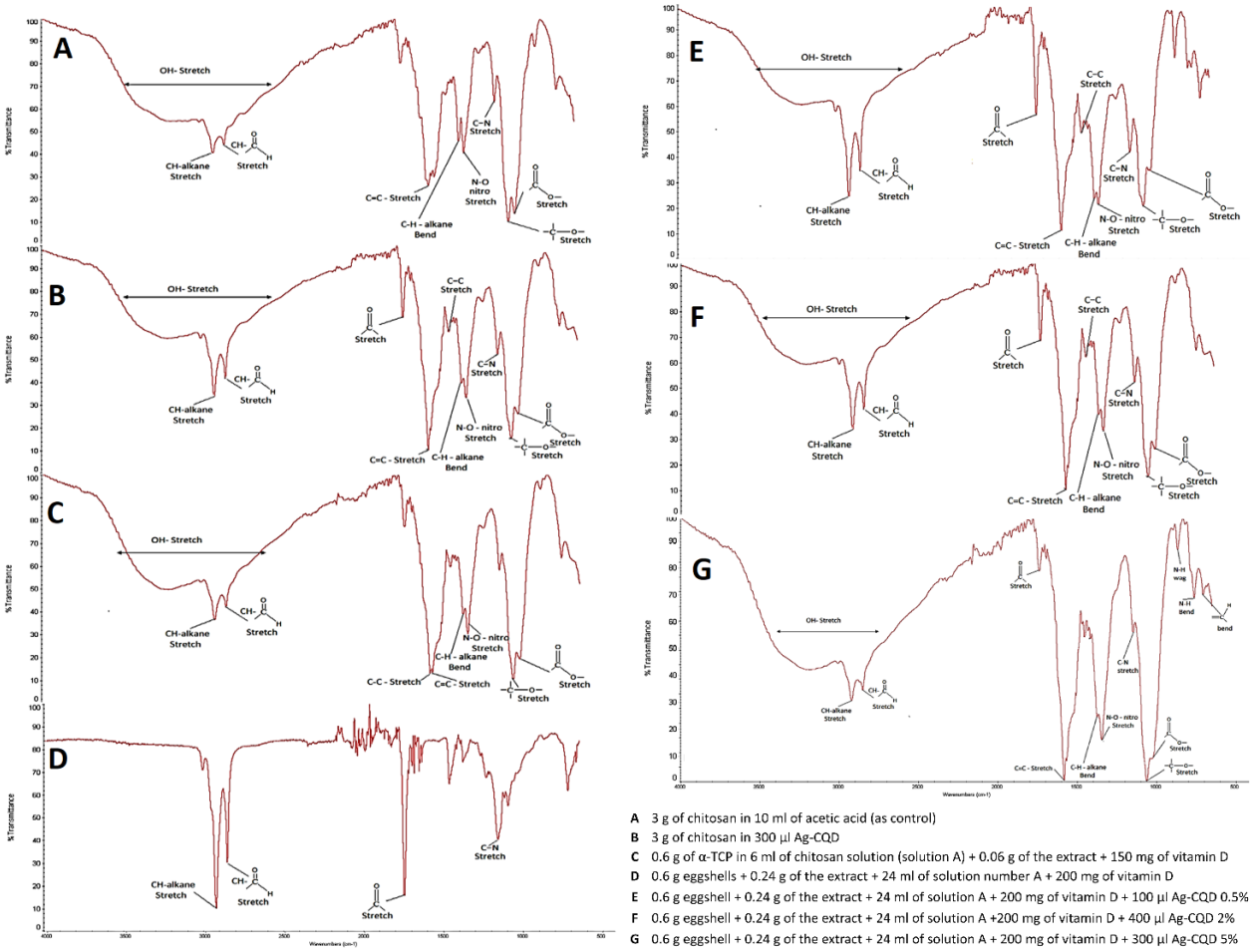

A 3 g of chitosan in 10 ml of acetic acid (as control)
B 3 g of chitosan in 300 µl Ag-CQD
C 0.6 g of α-TCP in 6 ml of chitosan solution (solution A) + 0.06 g of the extract + 150 mg of vitamin D
D 0.6 g eggshells + 0.24 g of the extract + 24 ml of solution number A + 200 mg of vitamin D
E 0.6 g eggshell + 0.24 g of the extract + 24 ml of solution A + 200 mg of vitamin D + 100 µl Ag-CQD 0.5%
F 0.6 g eggshell + 0.24 g of the extract + 24 ml of solution A +200 mg of vitamin D + 400 µl Ag-CQD 2%
G 0.6 g eggshell + 0.24 g of the extract + 24 ml of solution A + 200 mg of vitamin D + 300 µl Ag-CQD 5%

Figure 3. ATR-FTIR spectra of designed and synthesized scaffolds.

vated concentrations of Ag-CQDs (2% and 5%) significantly reduced cell viability owing to oxidative stress generated by nanoparticles. Histological examination of wound healing shown that the 0.5% Ag-CQD scaffold outperformed scaffolds with greater concentrations in tissue regeneration. On Day 4, the wounds had significant neutrophil infiltration. On day 8, neutrophil counts decreased, and new vasculature together with dermal-epidermal layers were seen, particularly in wounds treated with 0.5% Ag-CQD scaffolds (Fig. 5). Wounds treated with the 0.5% Ag-CQD scaffold on day 12 exhibited re-epithelialization, granulation tissue production, angiogenesis, and hair follicle growth, all of which signify successful wound healing.

The results indicated that three scaffolds, namely Vitamin D/Extract/Egg shell/CQD-Ag 0.5%, Vitamin D/Extract/Egg shell/CQD-Ag 2%, and Vitamin D/Extract/Egg shell/CQD-Ag 5%, were employed, and following the treatment duration, the regenerated tissue was examined to assess the level of improvement through Masson trichrome staining. The test findings indicated that on the fourth day of wound scaffold placement, a majority of neutrophils were present at the wound site, their aggregation termed granulosa, which indicated contamination of the area and a failure to initiate the healing stages. By the eighth day post-scaffold implantation, neutrophil levels significantly decline, blood vessels gradually emerge, and the epidermal and dermal layers become distinctly identifiable, particularly in scaffolds incorporating graphene oxide and henna extract. On the twelfth day, it is observed that the neutrophils have disappeared, and the repair phases are complete. In the sample with 0.5% CQD-Ag, the wound area has fully healed, angiogenesis has occurred, hair follicles have formed, and all layers of the skin are in final repair.

4. Discussions

This work concentrated on the development of bioactive nanofibrous scaffolds including VEGF, silver carbon quantum dots (Ag-CQD), Vitamin D, and *Lawsonia inermis* extract (henna) to synergistically promote antibacterial, antioxidant, and angiogenic effects for wound healing. Morphological study (SEM) revealed bead-free, homogeneous nanostructures with uniformly disseminated bioactive ingredients, which is crucial for guaranteeing reliable drug delivery. This is in accordance with recent advancements in the field, as discussed in a series of reports released over the past three years. Nanofibrous scaffolds have been extensively researched for their ability to mimic the extracellular matrix (ECM), providing mechanical support and enabling cell adhesion and growth. They were revealed in the recent past to be employed for more effective healing of wounds by means of better delivery of drugs, water retention, and tissue formation. Our uniform bead-free nanostructures scaffolds

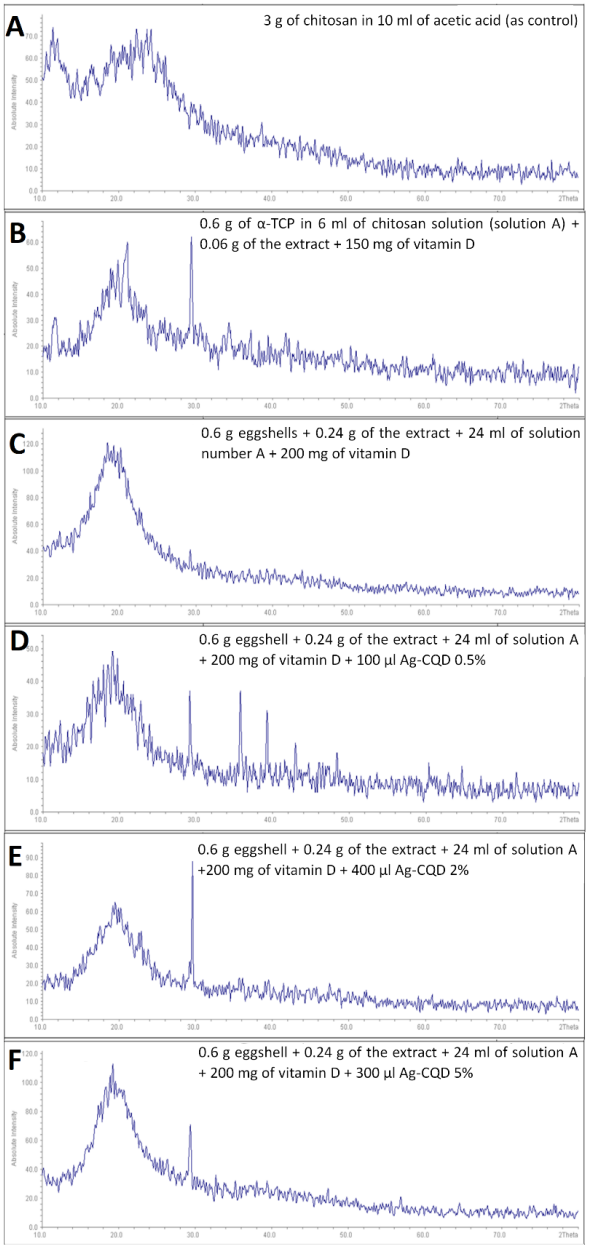

Figure 4. XRD spectra of designed and synthesized scaffolds.

ensure even drug delivery, as evidenced by these studies. The effective incorporation of Ag-CQD and plant extract was confirmed using FTIR and XRD analyses, and publications highlighted that the inclusion of nanomaterial structures significantly influences the release and functional stability of the material. Release experiments demonstrated a biphasic release of lawsone and VEGF, characterized by an initial burst release followed by a gradual release over time. However, optimal healing necessitates early modulation of initial inflammation, succeeded by tissue regeneration in the subsequent phase [25]. The continuous production of VEGF is particularly significant as it stimulates endothelial cell proliferation and neovascularization, essential for nutrition and oxygen transport throughout the tissue. This controlled release approach has been shown to greatly surpass the efficacy of free VEGF treatment, which is characterized by a short half-life and fast elimination [26]. The antibacterial activity shown significant suppression of both *E. coli* and *S. aureus*, affirming the strong antibacterial properties of Ag-CQDs and henna extract. The nanostructures containing 0.5% Ag-CQD exhibited the greatest antibacterial efficacy while maintaining fibroblast viability. This discovery aligns with other studies indicating that Ag-CQD loaded nanostructures may preferentially eradicate prokaryotic cells while sparing mammalian cells, potentially due to their capacity to generate oxidative stress in prokaryotes [27]. The *in vitro* scratch assay for cell migration demonstrated a significant enhancement in wound closure following treatment with VEGF-loaded nanostructures. The synergistic interaction of VEGF, Vitamin D, and lawsone extract likely played a crucial role in promoting fibroblast proliferation, regulating inflammation, and facilitating the remodeling of the extracellular matrix [28]. Vitamin D, known for its immunomodulatory effects, may have decreased pro-inflammatory cytokine levels, while the antioxidant capabilities of lawsone might have mitigated oxidative damage during wound healing. A highly important component of this study is the multifunctionality of the scaffold. The synergy of angiogenesis induction, antimicrobial activity, and antioxidant protection simultaneously addresses three of the most significant issues in wound care. This comprehensive method surpasses conventional wound dressings and singularly effective biomaterials that fail to fully promote tissue regeneration while also managing infections. Moreover, our method capitalizes on the intrinsic bioactivity of plant-derived constituents, which provide biocompatibility and reduced toxicity relative to synthetic additions [13]. While the findings are encouraging, it is important to emphasize that this study is confined to *in vitro* trials. The study requires augmentation through *in vivo* animal tests and clinical trials to assess the scaffold's behavior in biological environments. Enhancing the scaffold's mechanical characteristics and degradation rate might facilitate its clinical use. The findings of biphasic release of VEGF in the present study along with lawsone to further substantiate such results also show so. Our scaffolds' antibacterial activity through Ag-CQDs and henna extract also coincide with emerging evidence for the effective activity of nanoscaffolds with antimicrobial agents against prevalent wound pathogens. Besides, the antioxidant activity of henna extract in preventing oxidative stress in wound healing is consolidated by a study of the application of plant antioxidants to improve wound healing. Angiogenesis is a significant process engaged in wound healing, and endothelial cell growth and neovascularization observed with our scaffolds conform to more recent evidence to imply the involvement of angiogenic factors in tissue repair [25]. Our controlled release of VEGF from our scaffolds is a longer delivery system compared to free VEGF therapy, which has low half-life and high clearance rate. In comparison with recent studies, we can see some difference and similarity. Li et al. showed promoting angiogenesis with core–shell hydrogel/nanofiber composite scaffolds in diabetic wound healing [27]. Our investigation is prevalent in this objective but differs by utilizing more than one bioactive compound, e.g., Vitamin D and henna extract, to create more diversified therapeutic effects. Scientists inves-

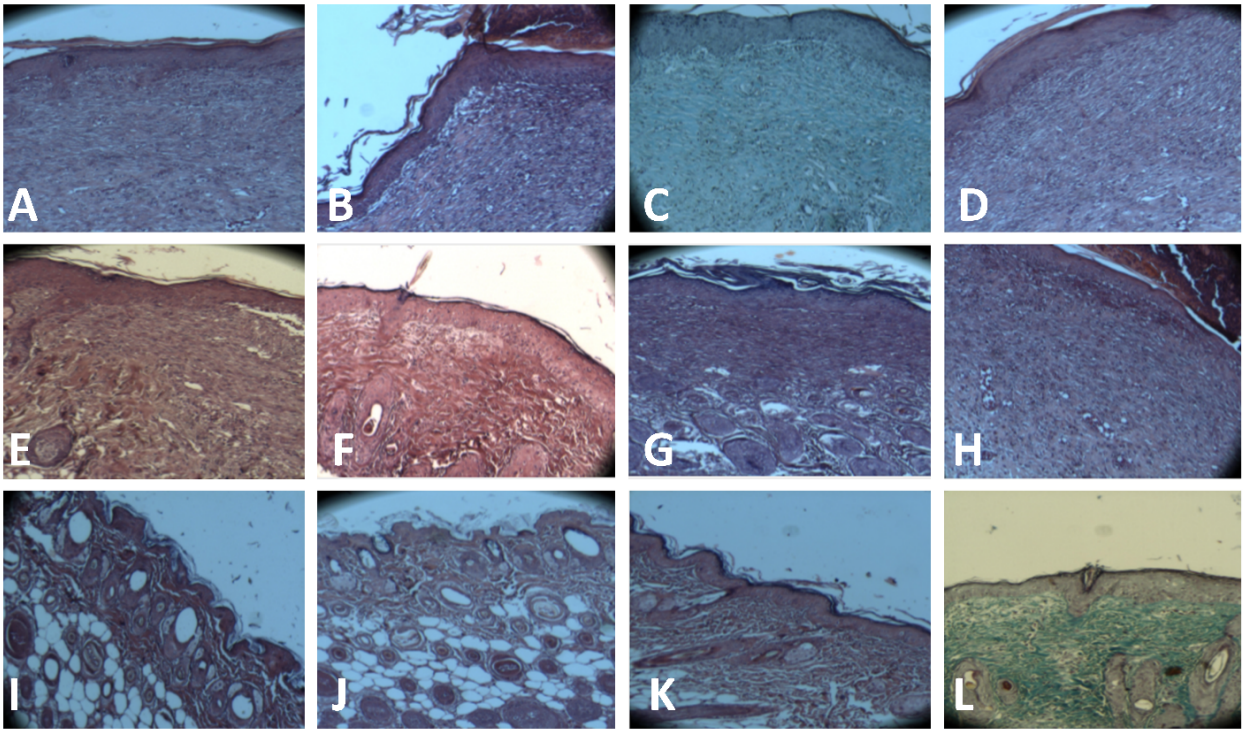

Figure 5. Tissues stained with Masson's trichrome stain of three scaffolds including eggshell extract, vitamin D and Ag-CQD at (B-F-J) 0.5%, (C-G-K) 2% and (D-H-L) 5% compared to the untreated control (A-E-I) after the end of the treatment period of four days (first row), eight days (middle row) and twelve days (bottom row) in order to measure the degree of improvement.

tigated electrospun nanofibers with nanoemulsion having antioxidant and antimicrobial properties for the healing of burns [29]. Our investigation, however, utilizes Ag-CQDs for enhanced antibacterial activity and VEGF for angiogenesis. Zhang et al. also reported increased angiogenesis and collagen synthesis in diabetic wounds with the application of bioglass sustained-release scaffolds but without the application of this study's multi-targeting strategy [30]. Our study's multi-perspective approach of VEGF, Ag-CQD, Vitamin D, and henna extract presents a one-stop solution for the primary challenges of healing diabetic wounds. While previous research has focused on isolated building blocks, our complete strategy is synergistic, enhancing the overall therapeutic potency. While our in vitro results are promising, more work is needed to ascertain the in vivo efficacy and clinical significance of these scaffolds. Tuning of the mechanical properties of the scaffolds and degradation rates should be the focus of future investigations to render them clinically relevant.

5. Conclusions

This research successfully developed and functionalized a multifunctional nanofibrous scaffold containing VEGF, Ag-CQDs, Vitamin D, and *Lawsonia inermis* extract, capable of promoting angiogenesis, exhibiting antibacterial properties, and mitigating oxidative stress to enhance wound healing. The scaffold possessed an appropriate nanostructure, facilitated the sustained release of bioactive compounds, exhibited exceptional antibacterial properties, and promoted fibroblast migration and proliferation. The combined action of the encapsulated compounds enhanced the scaffold's effectiveness. VEGF induced extensive angiogenic stimulation, Ag-CQDs conferred broad bacterial resistance, whereas lawsone and Vitamin D offered antioxidant properties and immunomodulatory effects. The cumulative impact of these medicines produced the necessary milieu for wound healing by facilitating tissue regeneration, enhancing infection resistance, and mitigating oxidative damage. This multifunctional scaffold offers more advantages than standard wound dressings by concurrently addressing many wound healing pathways. The findings of this work are critically significant for the advancement of innovative wound healing materials based on nanotechnology and bioactive agents. However, more *in vivo* investigations and clinical trials are required to ascertain the therapeutic potential of the scaffold, improve its features for therapeutic applications, and evaluate its safety and biocompatibility in human patients over an extended duration.

Acknowledgements
We thank the Shahid Beheshti University Council for their instrumentation and financial support.

Ethical Approval
This article is a continuation of previous study conducted by Prof. M. Omidi [31] and the receipt over ethical approval by Shahid Beheshti University of Medical Science NO. IR.SBMU. REC.1396.239).

Authors Contribution
FM: Conceptualization, Supervision, Methodology. AH: Data curation, Writing an original draft. HSAO: Data curation, formal analysis, and IF: Writing and editing the original draft.

Availability of data and materials
The datasets generated during and/or analyzed during the current study are available from the corresponding author on reasonable request.

Conflict of interests
The authors declare that they have no known competing financial interests or personal relationships that could have appeared to influence the work reported in this paper.

References

[1] M. M. Barker, M. J. Davies, F. Zaccardi, E. M. Brady, A. P. Hall, J. J. Henson, K. Khunti, A. Lake, E. L. Redman, A. V. Rowlands, J. Speight, T. Yates, J. A. Sargeant, and M. Hadjiconstantinou. Age at Diagnosis of Type 2 Diabetes and Depressive Symptoms, Diabetes-Specific Distress, and Self-Compassion. *Diabetes Care*, **46** (2):579–586, (2023).
DOI: https://doi.org/10.2337/dc22-1237.

[2] M. Edmonds, C. Manu, and P. Vas. The current burden of diabetic foot disease. *J Clin Orthop Trauma*, **17**:88–93, (2021).
DOI: https://doi.org/10.1016/j.jcot.2021.01.017.

[3] R. Keni, F. Begum, K. Gourishetti, G. L. Viswanatha, P. G. Nayak, K. Nandakumar, and R. R. Shenoy. Diabetic wound healing approaches: an update. *J Basic Clin Physiol Pharmacol*, **34**:137–150, (2022).
DOI: https://doi.org/10.1515/jbcpp-2021-0340.

[4] S. Jais. Various Types of Wounds That Diabetic Patients Can Develop: A Narrative Review. *Clinical Pathology*, **16**, (2023).
DOI: https://doi.org/10.1177/2632010X231205366.

[5] K. Zlobina, E. Malekos, H. Chen, and M. Gomez. Robust classification of wound healing stages in both mice and humans for acute and burn wounds based on transcriptomic data. . *BMC Bioinformatics*, **24**, (2023).
DOI: https://doi.org/10.1186/s12859-023-05295-z.

[6] F. Couic-Marinier. Wounds and advice in nutrition, aromatherapy and homoeopathy Plaies et conseils en nutrition, aromatherapie et homeopathie. *Actualites Pharmaceutiques*, **55**:30–33, (2016).
DOI: https://doi.org/10.1016/j.actpha.2016.01.006.

[7] M. Li, Q. Hou, L. Zhong, Y. Zhao, and X. Fu. Macrophage Related Chronic Inflammation in Non-Healing Wounds. *Front Immunol.*

[8] S. M. Aitcheson, F. D. Frentiu, S. E. Hurn, K. Edwards, and R. Z. Murray. Skin wound healing: Normal macrophage function and macrophage dysfunction in diabetic wounds. *Molecules*, **26**:1–11, (2021).
DOI: https://doi.org/10.3390/molecules26164917.

[9] A. Hassanshahi, M. Moradzad, S. Ghalamkari, M. Fadaei, A. J. Cowin, and M. Hassanshahi. Macrophage-Mediated Inflammation in Skin Wound Healing. *Cells*, **11**, (2022).
DOI: https://doi.org/10.3390/cells11192953.

[10] B. R. Freedman, C. Hwang, S. Talbot, B. Hibler, S. Matoori, and D. J. Mooney. Breakthrough treatments for accelerated wound healing. *Sci Adv.*, **9**:1–10.

[11] M. Sharifiaghdam, E. Shaabani, R. Faridi-Majidi, S. C. De Smedt, K. Braeckmans, and J. C. Fraire. Macrophages as a therapeutic target to promote diabetic wound healing. *Mol Ther*, **30**:2891–2908, (2022).
DOI: https://doi.org/10.1016/j.ymthe.2022.07.016.

[12] H. Y. H. Alimaml, W. A. Hussein, S. Ibrahim, S. Abdelgani, N. Alharthi, L. B. Eltayeb, S. A. Elmahdi, and A. E. A. Abdrabo. Blood Glucose, HbA1c Level, and its Correlation with VEGF-A (+405G/C) Polymorphism as Biomarker Predicts the Risk of Retinopathy and Nephropathy in Type 2 Diabetic Patients. . *Rep Biochem Mol Biol.*, **11**:421–429, (2022).
DOI: https://doi.org/10.52547/rbmb.11.3.421.

[13] H. E. Talbott, S. Mascharak, M. Griffin, D. C. Wan, and M. T. Longaker. Wound healing, fibroblast heterogeneity, and fibrosis. *Cell Stem Cell*, **22**(8):1161–1180, (2022).
DOI: https://doi.org/10.1016/j.stem.2022.07.006.

[14] S. Kaewsrisung, S. Sukpat, N. Issarasena, S. Patumraj, and J. Somboonwong. The effects of oral Aloe vera on the efficacy of transplanted human endothelial cells and the expression of matrix metalloproteinases in diabetic wound healing. *Heliyon*, **7**:e08533, (2021).
DOI: https://doi.org/10.1016/j.heliyon.2021.e08533.

[15] H. O. Elansary, A. Szopa, P. Kubica, H. Ekiert, F. A. Al-Mana, and M. A. Al-Yafrsi. Antioxidant and biological activities of acacia saligna and lawsonia inermis natural populations. *Plants*, **9**:1–17, (2020).
DOI: https://doi.org/10.3390/plants9070908.

[16] J. Zhang, H. Liu, T. Che, Y. Zheng, X. Nan, and Z. Wu. Nanomaterials for diabetic wound healing: Visualization and bibliometric analysis from 2011 to 2021. *Front Endocrinol (Lausanne)*, **14**:1–13, (2023).
DOI: https://doi.org/10.3389/fendo.2023.1124027.

[17] A. Yusuf Aliyu and O. A. Adeleke. Nanofibrous Scaffolds for Diabetic Wound Healing. *Pharmaceutics*, **15**, (2023).
DOI: https://doi.org/10.3390/pharmaceutics15030986.

[18] X. Ou, L. Guan, W. Guo, X. Zhang, S. Wu, D. Guo, R. Li, A. V. Zvyagin, Q. Lin, and W. Qu. Graphene oxide-based injectable conductive hydrogel dressing with immunomodulatory for chronic infected diabetic wounds. *Mater Des.*, **224**, (2022).
DOI: https://doi.org/10.1016/j.matdes.2022.111284.

[19] B. Eisazadeh, F. Mirzajani, and Y. Sefidbakht. How is the Effect of Silver Nanoparticles and Lipase/Cellulase Enzymes on Each Other? *Iran J Sci Technol Trans A Sci.*, **44**, (2020).
DOI: https://doi.org/10.1007/s40995-020-00820-8.

[20] M. Ghasemi, T. Turnbull, S. Sebastian, and I. Kempson. The mtt assay: Utility, limitations, pitfalls, and interpretation in bulk and single-cell analysis. *Int J Mol Sci.*, **22**:12827, (2021).
DOI: https://doi.org/10.3390/IJMS222312827/S1.

[21] S. Lenzen. The mechanisms of alloxan- and streptozotocin-induced diabetes. *Diabetologia*, **51**:216–226, (2008).
DOI: https://doi.org/10.1007/s00125-007-0886-7.

[22] M. Elsner, E. Gurgul-Convey, and S. Lenzen. Relative importance of cellular uptake and reactive oxygen species for the toxicity of alloxan and dialuric acid to insulin-producing cells. *Free Radic Biol Med.*, **41**:825–834, (2006).
DOI: https://doi.org/10.1016/j.freeradbiomed.2006.06.002.

[23] Y. Cheng, H. Kang, J. Shen, H. Hao, J. Liu, Y. Guo, Y. Mu, and W. Han. Beta-cell regeneration from vimentin + /MafB + cells after STZ-induced extreme beta-cell ablation. *Sci Rep.*

[24] F. Mirzajani, H. Askari, S. Hamzelou, M. Farzaneh, and A. Ghassempour. Effect of silver nanoparticles on *Oryza sativa* L. and its rhizosphere bacteria. *Ecotoxicol Environ Saf.*, **88**, (2013).
DOI: https://doi.org/10.1016/j.ecoenv.2012.10.018.

[25] H. Nosrati, R. Aramideh Khouy, A. Nosrati, M. Khodaei, M. Banitalebi-Dehkordi, K. Ashrafi-Dehkordi, S. Sanami, and Z. Alizadeh. Nanocomposite scaffolds for accelerating chronic wound healing by enhancing angiogenesis. *J Nanobiotechnology*, **19**: 33397416, (2021).
DOI: https://doi.org/10.1186/s12951-020-00755-7,.

[26] F. Shams, H. Moravvej, S. Hosseinzadeh, E. Mostafavi, H. Bayat, B. Kazemi, M. Bandehpour, E. Rostami, A. Rahimpour, and H. Moosavian. Overexpression of VEGF in dermal fibroblast cells accelerates the angiogenesis and wound healing function: *in vitro* and *in vivo* studies. *Sci Rep.*, **12**, (2022).
DOI: https://doi.org/10.1038/s41598-022-23304-8.

[27] T. Liu, Q. Pang, K. Mai, X. He, L. Xu, F. Zhou, and Y. Liu. Silver nanoparticle@carbon quantum dot composite as an antibacterial agent. *RSC Adv.*, **12**:9621, (2022).
DOI: https://doi.org/10.1039/D2RA00561A.

[28] F. Shams, H. Moravvej, S. Hosseinzadeh, E. Mostafavi, H. Bayat, B. Kazemi, M. Bandehpour, E. Rostami, A. Rahimpour, and H. Moosavian. Overexpression of VEGF in dermal fibroblast cells accelerates the angiogenesis and wound healing function: *in vitro* and *in vivo* studies. *Sci Rep.*, **12**, (2022).
DOI: https://doi.org/10.1038/s41598-022-23304-8.

[29] J. Li, T. Zhang, M. Pan, F. Xue, F. Lv, Q. Ke, and H. Xu. Nanofiber/hydrogel core–shell scaffolds with three-dimensional multilayer patterned structure for accelerating diabetic wound healing. *J Nanobiotechnology*, **20**, (2022).
DOI: https://doi.org/10.1186/S12951-021-01208-5.

[30] P. Zhang, Y. Jiang, D. Liu, Y. Liu, Q. Ke, and H. Xu. A bioglass sustained-release scaffold with ECM-like structure for enhanced diabetic wound healing. *Nanomedicine*, **15**:2241–2253, (2020).
DOI: https://doi.org/10.2217/NNM-2020-0053.

[31] A. Deilami, Z. Niknam, A. Golchin, V. Niazi, H. Zali, and M. Omidi. Novel hybrid scaffold for improving the wound repair process: evaluation of combined chitosan/eggshell/vitamin D scaffold for wound healing. *Polymer Bulletin*, **79**:3971–3986, (2022).
DOI: https://doi.org/10.1007/s00289-021-03692-z.